Dissociation Energies, Vibrational Frequencies, and ^{13}C NMR Chemical Shifts of the 18-Electron Species $[M(CO)_6]^n$ (M = Hf−Ir, Mo, Tc, Ru, Cr, Mn, Fe). A Density Functional Study

Andreas W. Ehlers,[†] Yosadara Ruiz-Morales,[‡] Evert Jan Baerends,[†] and Tom Ziegler*[,‡]

Afdeling Theoretische Chemie, Faculteit Scheikunde, Vrije Universiteit, De Boelelaan 1083, 1081 HV Amsterdam, The Netherlands, and Department of Chemistry, The University of Calgary, Calgary, Alberta, Canada T2N 1N4

Received February 26, 1997[⊗]

Density functional theory has been used to calculate dissociation energies, vibrational frequencies, and ^{13}C NMR chemical shifts of the following isoelectronic metal hexacarbonyls: $[Hf(CO)_6]^{2-}$, $[Ta(CO)_6]^-$, $W(CO)_6$, $[Re(CO)_6]^+$, $[Os(CO)_6]^{2+}$, $[Ir(CO)_6]^{3+}$; $Mo(CO)_6$, $[Tc(CO)_6]^+$, $[Ru(CO)_6]^{2+}$; and $Cr(CO)_6$, $[Mn(CO)_6]^+$, $[Fe(CO)_6]^{2+}$. The first CO ligand dissociation energy ΔH follows the ordering Ir > Re ∼ Os > Hf ∼ Ta ∼ W through the third transition series. A decomposition of ΔH into contributions from the CO to metal σ-donation and metal to CO π-back-donation reveals that this trend is the result of a stronger σ-donation in the more oxidized systems. An increase in ΔH toward higher oxidation state is also apparent for the limited sample of 3d and 4d systems. Within a triad, the 4d metal forms the weakest M−CO bond. The calculated CO stretching frequencies are in good agreement with experiment. Further, CO stretching frequencies, optimized R(C−O) distances, and the calculated contribution to ΔH from the π-back-donation all reveal the expected decline in π-back-donation toward the more positively charged systems. Both experimental and calculated ^{13}C NMR chemical shifts diminish with increasing oxidation state. It was shown that the stretch of CO on coordination and π-back-donation have positive (paramagnetic) contributions to the chemical shift, δ, whereas σ-donation has a negative (paramagnetic) contribution to δ. All factors contribute to the decline in δ with increasing oxidation state, although π-back-donation is predominant.

Introduction

The neutral hexacarbonyls $M(CO)_6$ (M = Cr, Mo, W) have been studied[1a−c] extensively. These studies have provided a detailed picture of periodic trends in the electronic structure of $M(CO)_6$ for M = Cr, Mo, W. Quite recently, Aubke[2] et al. synthesized a number of new 18-electron binary hexacarbonyls. By now, the scope of known species include $[Hf(CO)_6]^{2-}$, $[Ta(CO)_6]^-$, $W(CO)_6$, $[Re(CO)_6]^+$, $[Os(CO)_6]^{2+}$, $[Ir(CO)_6]^{3+}$ as well as $Mo(CO)_6$, $[Tc(CO)_6]^+$, $[Ru(CO)_6]^{2+}$ and $Cr(CO)_6$, $[Mn(CO)_6]^+$, $[Fe(CO)_6]^{2+}$.

The objective of the present study is to expand our understanding of periodic trends in the electronic structure of hexacarbonyls by theoretical investigations of the species newly synthesized by Aubke[2] et al. The extended series of compounds makes it possible not only to monitor changes within a triad but also to probe variations along a transition series. Our theoretical study will be based on density functional theory[3] (DFT) and include calculations on the first M−CO dissociation energy, CO vibrational frequencies, and optimized R(M−CO) and R(C−O) distances as well as ^{13}C NMR chemical shifts.

Computational Details

All calculations were based on the Amsterdam density functional package ADF.[4] This program has been developed by Baerends[4a,b] et al. and vectorized by Ravenek.[4e] The adopted numerical integration scheme was that developed by te Velde[4f,g] et al.

The metal centers were described by an uncontracted triple-ζ STO basis set[5,6] for the outer ns, np, nd, $(n + 1)$s, and $(n + 1)$p orbitals whereas the shells of lower energy were treated by the frozen core approximation.[4a] The valence on carbon and oxygen included the 1s shell and was described by an uncontracted triple-ζ STO basis augmented by a single 3d and 4f function, corresponding to basis set V of the ADF package.[4] A set of auxiliary[7] s, p, d, f, and g STO

[†] Vrije Universiteit.

[‡] The University of Calgary.

[⊗] Abstract published in *Advance ACS Abstracts,* October 1, 1997.

(1) (a) Ehlers, A. W.; Frenking, G. *J. Chem. Soc., Chem. Commun.* **1993**, 1709. (b) Ehlers, A. W.; Frenking, G. *J. Am. Chem. Soc.* **1994**, *116*, 1514. (c) Li, J.; Schreckenbach, G.; Ziegler, T. *J. Am. Chem. Soc.* **1995**, *117*, 486. (d) Rosa, A; Ehlers, A. W.; Baerends, E. J.; Snijders, J. G.; te Velde, G *J. Phys. Chem.* **1996**, *100*, 5690. (e) Baerends, E. J.; Rozendaal, A. *NATO ASI Ser.* **1986**, *C176*, 159. (f) Fan, L.; Ziegler, T. *J. Chem. Phys.* **1991**, *95*, 7401. (g) Li, J.; Schreckenbach, G.; Ziegler, T. *J. Phys. Chem.* **1994**, *98*, 4838.

(2) (a) Wang, C.; Bley, B.; Balzer-Jöllenbeck, G.; Lewis, A. R.; Siu, S. C.; Willner, H.; Aubke, F. *J. Chem. Soc., Chem. Commun.* **1995**, 2071. (b) Aubke, F. Unpublished results. (c) Bley, B.; Willner, H.; Aubke, F. *Inorg. Chem.* **1997**, *36*, 158. (d) Bach, C.; Willner, H.; Wang, C.; Rettig, S. J.; Trotter, J.; Aubke, F. *Angew. Chem., Int. Ed. Engl.* **1996**, *35*, 1974.

(3) (a) Ziegler, T. *Chem. Rev.* **1991**, *91*, 651. (b) Ziegler, T. *Can. J. Chem.* **1995**, *73*, 743.

(4) (a) Baerends, E. J.; Ellis, D. E.; Ros, P. *Chem. Phys.* **1973**, *2*, 41. (b) Baerends, E. J.; Ros, P. *Chem. Phys.* **1973**, *2*, 52. (c) Baerends, E. J.; Ros, P. *Int. J. Quantum Chem. Symp.* **1978**, *12*, 169. (d) te Velde, G. *Amsterdam Density Functional (ADF), User Guide, Release 1.1.3*; Department of Theoretical Chemistry, Free University: Amsterdam, The Netherlands, 1994. (e) Ravenek, W. In *Algorithms and Applications on Vector and Parallel Computers*; te Riele, H. J. J., Dekker, T. J., van de Horst, H. A., Eds.; Elsevier: Amsterdam, The Netherlands, 1987. (f) Boerrigter, P. M.; te Velde, G.; Baerends, E. J. *Int. J. Quantum Chem.* **1988**, *33*, 87. (g) te Velde, G.; Baerends, E. J. *J. Comput. Chem.* **1992**, *99*, 84. (h) Fonseca, C.; Visser, O.; Snijders, J. G.; te Velde, G.; Baerends, E. J. In *Methods and Techniques in Computational Chemistry, METECC-95*; Clementi, E., Corongiu, G., Eds.; ESCOM: Leiden, The Netherlands, 1995; p 307.

(5) Snijders, J. G.; Baerends, E. J.; Vernoijs, P. *At. Nucl. Data Tables* **1982**, *26*, 483.

(6) Vernooijs, P.; Snijders, J. G.; Baerends, E. J. *Slater Type Basis Functions for the Whole Periodic System*; Internal Report (in Dutch); Department of Theoretical Chemistry, Free University: Amsterdam, The Netherlands, 1981.

S0020-1669(97)00223-1 CCC: $14.00

Table 1. Bond Lengths (Å) and Selected Vibrational Frequencies[d] (cm^{-1}) of the Transition Metal Hexacarbonyls[a] $[M(CO)_6]^n$

	R(M−C)	R(C−O)	$\nu(a_{1g})$	$\nu(e_g)$	$\nu(t_{1u})$
$Hf(CO)_6^{2-}$	2.203	1.183	1902	1777	1767 (1757)
$Ta(CO)_6^-$	2.121 (2.083[f])	1.167 (1.149[f])	2029	1915	1896 (1850)
$W(CO)_6$	2.066 (2.058[b])	1.152 (1.141)	2116 (2126[c])	2019 (2021[c])	1998 (1998[c])
$Re(CO)_6^+$	2.058	1.139	2180 (2197)	2102 (2122)	2069 (2085)
$Os(CO)_6^{2+}$	2.047	1.127	2260 (2259)	2212 (2218)	2189 (2190)
$Ir(CO)_6^{3+}$	2.053	1.121	2300 (2295)	2272 (2276)	2252 (2254)
$Mo(CO)_6$	2.070 (2.063[b])	1.152 (1.145)	2109 (2121[c])	2017 (2025[c])	1997 (2003[c])
$Tc(CO)_6^+$	2.028	1.138	2179	2113	2092
$Ru(CO)_6^{2+}$	2.033	1.127	2248 (2254)	2206 (2222)	2187 (2199)
$Cr(CO)_6$	1.906 (1.914[b])	1.153 (1.140)	2105 (2119[c])	2015 (2027[c])	1993 (2000[c])
$Mn(CO)_6^+$	1.886	1.139	2176	2109	2090 (2090[e])
$Fe(CO)_6^{2+}$	1.895	1.129	2228 (2241)	2192 (2220)	2176 (2204)

[a] Experimental data are given in parentheses. [b] Reference 17a. [c] Reference 17b. [d] Experimental frequencies for charged species; refs 2a−2d. [e] Reference 17c. [f] Reference 17d.

functions, centered on all nuclei, was used to fit the molecular density and present Coulomb and exchange potentials accurately in each SCF cycle.

The self-consistent DFT calculations were carried out by augmenting the local exchange-correlation potential due to Vosko[8] et al. with Becke's[9] nonlocal exchange corrections and Perdew's[10] nonlocal correlation correction (NL-SCF). The chemical shift calculations of 3d and 4d complexes were treated without relativistic effects whereas quasi-relativistic[11] (NL-SCF+QR) calculations were carried out for the 5d complexes. Details of the GIAO-DFT method used in the chemical shift calculations have been described previously.[14] The inclusion of the frozen core approximation[12] and quasi-relativistic[13] effects in the shielding calculations will be described elsewhere.[14a] All the structures were optimized and vibrational frequencies were calculated by numerical differentiation of the analytical energy gradients at the NL-SCF+QR level.

The first bond dissociation energy (FBDE) of $[M(CO)_6]^n$ corresponds to the reaction enthalpy of the process

$$[M(CO)_6]^n \rightarrow [M(CO)_5]^n + CO$$
$$n = 2-, 1-, 0, 1+, 2+, 3+ \qquad (1)$$

(n represents the charge)

The DFT-calculated values reported in this work represent the electronic contribution to the reaction enthalpy of eq 1. The first ligand dissociation energy can be decomposed with the help of the extended transition state (ETS)[15] method as

$$\Delta H = \Delta E_{prep} + \Delta E^\circ + \Delta E_\sigma + \Delta E_\pi \qquad (2)$$

Here ΔE° is the steric interaction energy between CO and the $[M(CO)_5]^n$ fragment whereas ΔE_σ represents the contribution to ΔH due to the donation from σ_{CO} to the LUMO of $[M(CO)_5]^n$ and ΔE_π is the contribution to ΔH due to the back-donation from the HOMO of $[M(CO)_5]^n$ to the π_{CO}* orbital of CO. The last term, ΔE_{prep}, is the energy required to relax the structures of the free fragments to the geometries they adopt in the combined $[M(CO)_6]^n$ complex. A more detailed description of the ETS scheme and its applications to metal carbonyls can be found elsewhere.[16]

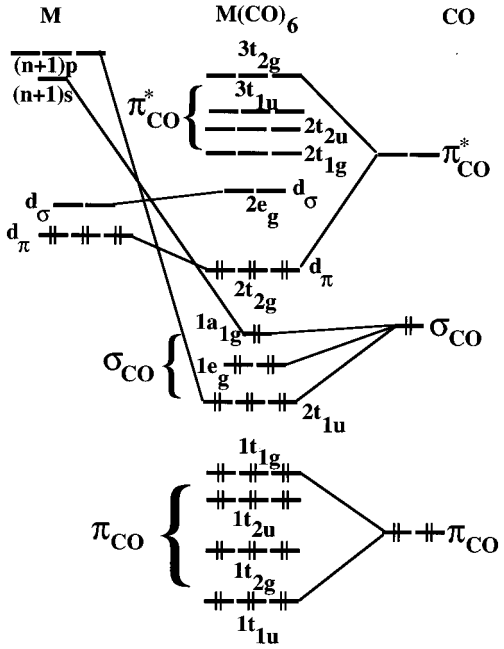

Figure 1. Schematic orbital level diagram for $M(CO)_6$.

We summarize in Figure 1 the well-known orbital level diagram of $M(CO)_6$ for later reference. The molecular orbitals are composed of π_{CO}*, π_{CO}, and σ_{CO} on the CO ligands and nd_π, $(n+1)$s, and $(n+1)$p on the metal. The HOMO $2t_{2g}$ and LUMO $2e_g$ are primarily nd-based orbitals.

Result and Discussion

Bond Distances. Table 1 provides optimized R(M−CO) and R(C−O) distances for all the hexacarbonyls under investigation along with the few experimental estimates.[17a] Table 2 displays

(7) Krijn, J.; Baerends, E. J. *Fit Functions in the HFS Method*; Internal Report (in Dutch); Department of Theoretical Chemistry, Free University: Amsterdam, The Netherlands, 1984.
(8) Vosko, S. H.; Wilk, L.; Nusair, M. *Can. J. Phys.* **1980**, *58*, 1200.
(9) Becke, A. *Phys. Rev. A* **1988**, *38*, 3098.
(10) Perdew, J. *Phys. Rev. B* **1986**, *33*, 8822.
(11) (a) Snijders, J. G.; Baerends, E. J. *Mol. Phys.* **1978**, *36*, 1789. (b) Snijders, J. G.; Baerends, E. J.; Ros, P. *Mol. Phys.* **1979**, *38*, 1909. (c) Ziegler, T.; Tschinke, V.; Baerends, E. J.; Snijders, J. G.; Ravenek, W. *J. Phys. Chem.* **1989**, *93*, 3050. (d) Pyykkö, P. *Chem. Rev.* **1988**, *88*, 563.
(12) Schreckenbach, G.; Ziegler, T. *Int. J. Quantum Chem.* **1996**, *60*, 753.
(13) Schreckenbach, G.; Ziegler, T. *Int. J. Quantum Chem.* **1997**, *61*, 899.
(14) (a) Schreckenbach, G.; Ziegler, T. *J. Phys. Chem.* **1995**, *99*, 606. (b) Schreckenbach, G.; Dickson, R. M.; Ruiz-Morales, Y.; Ziegler, T. In *Density Functional Theory in Chemistry*; Laird, B., Ross, R., Ziegler, T., Eds.; American Chemical Society: Washington, DC, 1996. (c) Ruiz-Morales, Y.; Schreckenbach, G.; Zielger, T. *J. Phys. Chem.* **1996**, *100*, 3359. (d) Schreckenbach, G.; Ruiz-Morales, Y.; Ziegler, T. *J. Chem. Phys.* **1996**, *104*, 8605. (e) Ruiz-Morales, Y.; Schreckenbach, G.; Ziegler, T. *Organometallics* **1996**, *15*, 3920. (f) Kaupp, M.; Malkin, V. G.; Malkina, O. L.; Salahub, D. R. *Chem. Eur. J.* **1996**, *2*, 24.
(15) (a) Ziegler, T.; Rauk, A. *Theor. Chim. Acta* **1977**, *46*, 1. (b) Ziegler, T. *NATO ASI Ser.* **1986**, *C176*, 189. (c) Ziegler, T.; Tschinke, V.; Ursenbach, C. *J. Am. Chem. Soc.* **1987**, *109*, 4825. (d) Ziegler, T. *NATO ASI Ser.* **1992**, *C378*, 367.
(16) Ziegler, T.; Tschinke, V.; Ursenbach, C. *J. Am. Chem. Soc.* **1987**, *109*, 4825.
(17) (a) Arnesen, S. P.; Seip, H. M. *Acta Chem. Scand.* **1966**, *20*, 2711. (b) Jones, L. H.; McDowell, R. S.; Goldblatt, M. *Inorg. Chem.* **1969**, *8*, 2349. (c) Kruck, T.; Noack, M. *Chem. Ber.* **1969**, *8*, 2349. (d) Calderazzo, F.; Englert, U.; Pamploni, G.; Pelizzi, G.; Zamboni, R. *Inorg. Chem.* **1983**, *22*, 1865.

Table 2. Calculated Hirshfeld Charges[a] of the Third-Row Transition Metal Hexacarbonyls, $[M(CO)_6]^n$

	M	C	O
$Hf(CO)_6^{2-}$	−0.168	−0.059	−0.246
$Ta(CO)_6^{-}$	−0.063	+0.015	−0.171
$W(CO)_6$	+0.036	+0.088	−0.094
$Re(CO)_6^{+}$	+0.118	+0.155	−0.009
$Os(CO)_6^{2+}$	+0.141	+0.218	+0.092
$Ir(CO)_6^{3+}$	+0.205	+0.275	+0.191

[a] For a definition, see ref 18.

effective nuclear charges based on the population analysis due to Hirshfeld[18] for the 5d series.

We might consider $[Hf(CO)_6]^{2-}$ and $[Ta(CO)_6]^{-}$ as generated from $W(CO)_6$ by removing respectively one and two protons from the tungsten nucleus. The removal will reduce the effective nuclear charge on the metal and expand the radial extent of the valence 5d orbitals, resulting in an elongation of the R(M−CO) distance, Table 1. The reduced effective charge will further cause a flow of density to the CO ligands and the π^*_{CO} orbital, thus causing a stretch of the R(C−O) distance, Table 1. It follows from Table 2 that the metal center remains nearly neutral and that a substantial amount of charge ends up on the more electronegative oxygen atom, Table 2.

We can generate $[Re(CO)_6]^{+}$, $[Os(CO)_6]^{2+}$, and $[Ir(CO)_6]^{3+}$ from $W(CO)_6$ by subsequently adding a proton to the metal center and increase the effective nuclear charge. The result is now a flow of density from the CO ligands and the π^*_{CO} orbital to the metal center. As a consequence, the R(C−O) distance is seen to contract with a growing positive charge on the metal complex. One might also have expected a contraction of the 5d orbitals and the R(M−CO) distance as the effective nuclear charge increases on the metal center with additional protons. The R(M−CO) distance does decrease compared to R(W−CO), but not by much. This is primarily because the attraction of the additional protons is reduced by an increase in the screening of the core electrons as their orbitals are contracted. It follows from Table 2 that the flow of density comes from both carbon and oxygen. The flow is seen to keep the nucleus nearly neutral. We find much the same trends in the R(M−CO) and R(C−O) distances for the 4d series $[Mo(CO)_6]$, $[Tc(CO)_6]^{+}$, $[Ru(CO)_6]^{2+}$ and 3d series $[Cr(CO)_6]$, $[Mn(CO)_6]^{+}$, $[Fe(CO)_6]^{2+}$, Table 1.

Vibrational Frequencies. One of the two primary methods of characterization for the hexacarbonyls synthesized by Aubke et al. has been vibrational spectroscopy.[2] The calculated and experimental CO stretching frequencies for the isoelectronic metal carbonyls are summarized in Table 1. Raman spectra for $[Hf(CO)_6]^{2-}$, $[Ta(CO)_6]^{-}$, and $[Mn(CO)_6]^{+}$ are not reported in the literature and there are no experimental vibrational frequencies recorded for $[Tc(CO)_6]^{+}$. Most of the calculated vibrational frequencies agree with experiment to within 1−25 cm^{-1}. The $[Ta(CO)_6]^{-}$ complex presents the largest discrepancy between experiment and theory with a deviation of 46 cm^{-1}. It has been found that an accurate reference geometry is one of the most important requirements for good estimates of vibrational frequencies.[19] We estimate that the small deviations in the CO stretching frequencies translate into errors of ±0.01 Å in the calculated R(C−O) distances.

The calculated and experimental trend from left to right along the three transition series is as expected an increase in the CO stretching frequencies as the π-back-donation is reduced by an increase in the formal metal oxidation state, Table 1. The CO stretching frequencies within a triad are quite similar for modes of the same symmetry. Thus, it is not easy to use these properties to deduce information about differences in the bonding mode within a homologous series of 3d, 4d, and 5d hexacarbonyls.

Table 3. First Bond Dissociation Energies and Bond Energy Decomposition[a] (kcal/mol)

	FBDE (ΔH)	$\Delta E^\circ + \Delta E_{prep}$	ΔE_σ	ΔE_π
$Hf(CO)_6^{2-}$	53.3	−23.5	22.8	54.0
$Ta(CO)_6^{-}$	49.3	−29.0	29.1	49.2
$W(CO)_6$	46.0	−31.1	35.8	41.3
$Re(CO)_6^{+}$	51.2	−30.9	47.3	34.8
$Os(CO)_6^{2+}$	62.6	−29.0	62.4	29.2
$Ir(CO)_6^{3+}$	76.4	−28.2	76.5	28.1
$Mo(CO)_6$	39.9	-28.6	30.9	37.6
$Tc(CO)_6^{+}$	42.1	−27.6	40.0	29.7
$Ru(CO)_6^{2+}$	50.8	−24.9	51.3	24.4
$Cr(CO)_6$	43.1	−31.7	34.7	40.1
$Mn(CO)_6^{+}$	44.8	−30.2	44.3	30.7
$Fe(CO)_6^{2+}$	53.0	−26.5	54.8	24.7

[a] FBDE (ΔH) = $\Delta E^\circ + \Delta E_{prep} + \Delta E_\sigma + \Delta E_\pi$.

Bond Dissociation Energies. Calculated values for the first M−CO bond dissociation energy, ΔH, are presented in Table 3. Also shown is the decomposition of ΔH into the term ΔE_σ representing the σ-donation and the term ΔE_π representing the π-back-donation. As expected, the σ-donation contribution ΔE_σ increases and the π-back-donation ΔE_π decreases from left to right in each of the three transition metal series.

For the neutral and negatively charged species, the π-back-donation, ΔE_π, is more important than σ-donation, ΔE_σ. Further, the increase in the π-back-donation through the series $W(CO)_6$, $[Ta(CO)_6]^{-}$, and $[Hf(CO)_6]^{2-}$ is seen to cause a corresponding increase in the M−CO dissociation energy ΔH, Table 3. On the other hand, for the positively charged complexes, ΔE_σ becomes the predominant term, especially among the 5d complexes. Combined ΔH is seen to increase with ΔE_σ in each of the three series from the neutral species toward the more positively charged complex.

Within the chromium triad, ΔH follows the order Mo < Cr < W with the 4d member forming the most labile bond. The W−CO bond is strengthened compared to the corresponding Mo−CO bond by a relativistic destabilization[1c] of the 5d levels, which enhances the π-back-donation in the case of tungsten.

We notice as well, for the group 7 and group 8 triads, that the 4d congener forms the weakest bond whereas the M−CO bond is strongest for the 5d member. In this case, the calculated enhancement of the π-back-donation is of little importance for the stronger Os−CO and Ir−CO bonds, Table 3. Instead, the σ-donation, ΔE_σ, is increased by a relativistic stabilization of the 6s and 6p orbitals, which makes the σ-interactions in $1a_{1g}$ and $2t_{1u}$ of Figure 1 stronger. Relativistic effects are in general more important for the heavier 5d homologue.[11d]

NMR Chemical Shifts. The second primary method of characterization for the hexacarbonyls synthesized by Aubke et al.[2] has been NMR spectroscopy. Tables 4 and 5 display calculated and experimental[2] ^{13}C chemical shifts for the octahedral metal carbonyls. The theoretical chemical shifts δ have further been decomposed into paramagnetic, δ^p, and diamagnetic, δ^d, components. The calculated and observed chemical shifts exhibit the same decrease in the chemical shift toward the more oxidized species along each of the three transition series. Within a triad, the shifts decrease toward the heavier congener. On top of shortcomings of our theory, the deviations between experiment and theory can be attributed to the influence of thermal motion and for the ionic species also

(18) (a) Hirshfeld, F. L. *Theor. Chim. Acta* **1977**, *44*, 129. (b)Wiberg, K. B.; Rablen, P. R. *J. Comput. Chem.* **1993**, *14*, 1504.
(19) (a) Berces, A.; Ziegler, T. *J. Phys..Chem* **1995**, *99*, 11417. (b) Bérces A. *J. Phys. Chem.* **1996**, *100*, 16538.

Table 4. Calculated and Experimental Chemical Shifts for Various $[M(CO)_6]^n$ 5d Complexes

system	R(C−O), Å	exptl chem shift δ, ppm[d]	calcd[c] chem shift δ, ppm	calcd diamagnetic chem shift δ^d, ppm	calcd paramagnetic chem shift δ^p, (ppm)
$[Hf(CO)_6]^{2-}$ [b]	1.183[a]	244	228.3	−8.7	237.0
$[Ta(CO)_6]^-$ [b]	1.167[a]	211	211.8	−11.4	223.2
$W(CO)_6$ [b]	1.152[a]	192	197.7	−11.6	209.3
$[Re(CO)_6]^+$ [b]	1.139[a]	171	183.9	−12.4	196.3
$[Os(CO)_6]^{2+}$ [b]	1.127[a]	147	172.4	−14.5	186.9
$[Ir(CO)_6]^{3+}$ [b]	1.121[a]	121	153.6	−15.2	168.8

[a] Optimized structure. [b] Relativistic NL-SCF-QR calculations. [c] Calculated absolute chemical shielding $\sigma_{TMS} = 179.5$ ppm, $\sigma^d = 250.24$, $\sigma^p = -70.78$ and $\delta = \sigma_{TMS} - \sigma_{substance}$. [d] Reference 2d.

Table 5. Calculated and Experimental Chemical Shifts for Various $[M(CO)_6]^n$ Complexes of 3d and 4d Elements

system	R(C−O), Å	exptl chem shift δ, ppm	calcd[b] chem shift δ, ppm	calcd diamagnetic chem shift δ^d, ppm	calcd paramagnetic chem shift, δ^p, (ppm)
$Mo(CO)_6$	1.152[a]	203.0[g]	203.4[c]	−13.9	217.3
$[Tc(CO)_6]^+$	1.138[a]		193.1	−15.2	208.3
$[Ru(CO)_6]^{2+}$	1.127[a]	166.1[d]	178.6	−16.5	195.1
$Cr(CO)_6$	1.153[a]	212.0[g]	207.2[c]	−12.2	219.4
$[Mn(CO)_6]^+$	1.139[a]	195.0[e]	198.0	−13.7	211.7
$[Fe(CO)_6]^{2+}$	1.129[a]	179.0[f]	182.3	−13.9	196.2

[a] Optimized structure. [b] Calculated absolute chemical shielding $\sigma_{TMS} = 179.5$ ppm, $\sigma^d = 250.24$, $\sigma^p = -70.78$, and $\delta = \sigma_{TMS} - \sigma_{substance}$. [c] Reference 14c. [d] Reference 2a. [e] Reference 2b. [f] Reference 2c. [g] Reference 21.

Table 6. Contribution to the Calculated Shift[a] in the Isotropic Shielding of ^{13}C for Complexed CO in $[M(CO)_6]^n$ for Various 5d Systems

system	$\Delta\delta^{dist}_{xx}$, ppm[b]	$\Delta\delta^{dist}_{yy}$, ppm[b]	$\Delta\delta^{dist}_{zz}$, ppm[b]	$\Delta\delta^{p'}_{xx}$, ppm[d]	$\Delta\delta^{p'}_{yy}$, ppm[d]	$\Delta\delta^{p'}_{zz}$, ppm[d]	$\Delta\delta^{oc}$, ppm[e]	$\Delta\delta^{oc-vir}$, ppm[f]	$\Delta\delta$, ppm[a]	energy gap, eV $2t_{2g} \rightarrow 2t_{1g}$
$[Hf(CO)_6]^{2-}$	31.6[c]	31.6	0.0	−14.1	−14.3	103.6	−5.8	46.2	40.4	3.406
$[Ta(CO)_6]^-$	21.9[c]	21.9	0.0	−15.0	−15.0	60.2	−0.8	24.7	23.9	4.262
$W(CO)_6$	13.7[c]	13.7	0.0	−19.9	−19.9	26.5	5.1	4.7	9.8	5.506
$[Re(CO)_6]^+$	6.3[c]	6.3	0.0	−26.8	−26.9	14.7	4.8	−8.8	−4.0	6.613
$[Os(CO)_6]^{2+}$	−0.4[c]	−0.4	0.0	−34.9	−34.9	10.6	4.5	−20.0	−15.5	7.322
$[Ir(CO)_6]^{3+}$	−3.9[c]	−3.9	0.0	−54.7	−54.7	5.8	2.8	−37.1	−34.3	8.842

[a] Coordination shielding: $\Delta\delta = \sigma_{CO} - \sigma_{[M(CO)_6]^n}$ or $\Delta\delta = \Delta\delta^{oc} + {}^1/_3\sum_{s=1}^3 \Delta\delta^{dist}_{ss} + {}^1/_3\sum_{s=1}^3 \Delta\delta^{p'}_{ss}$. [b] $\Delta\vec{\delta}^{dist} = \vec{\sigma}^{p'}_{CO} - \vec{\sigma}^{p'}_{CO*}$. Here CO is the free CO molecule and CO* the distorted ligand with the bond length it will have in the complex. [c] Relativistic NL-SCF-QR calculations. [d] $\Delta\delta^{p'}_{ss} = \sigma^{p'}_{ss,CO*} - \sigma^{p'}_{ss,[M(CO)_6]^n}$ is the difference in the paramagnetic shielding between $[M(CO)_6]^n$, $\sigma^{p'}_{ss,[M(CO)_6]^n}$, and the distorted ligand CO*, $\sigma^{p'}_{ss,CO*}$. [e] $\Delta\delta^{oc}$ is the contribution to the coordination shielding $\Delta\delta$ from all the terms that only depend on the occupied orbitals. [f] $\Delta\delta^{oc-vir}$ is the contribution to the coordination shielding $\Delta\delta$ from the term that couples occupied and virtual orbitals.

to solvation effects. We note that it is the paramagnetic contribution, δ^p, that determines the total chemical shift, δ, whereas the diamagnetic part, δ^d, by comparison is numerically negligible and nearly constant, Tables 4 and 5. This is in accord with previous calculations[14c,f] on ^{13}C chemical shifts of metal carbonyls.

Complexation of a ligand to a metal is accompanied by changes in the chemical shifts of the ligand atoms. These effects are usually analyzed in terms of the coordination chemical shift.[14c] The coordination shift is defined as

$$\Delta\delta = \delta_{complex} - \delta_{ligand} \tag{3}$$

In our attempts at a quantitative interpretation of the trends in Tables 4 and 5, the shielding terminology (σ) is employed instead of the chemical shift (δ). Given the opposite signs of σ (shielding) and δ (chemical shift), the coordination shift should be defined in terms of the shielding terminology as

$$\Delta\delta = \sigma_{ligand} - \sigma_{complex} \tag{4}$$

Thus, the coordination shift is defined as the difference in the shielding of the free ligand and the shielding of the ligand in the complex.

The coordination shift $\Delta\delta$ has contributions from the paramagnetic coupling between occupied and virtual orbitals, $\Delta\delta^{oc-vir}$, as well as contributions, $\Delta\delta^{oc}$, that only depend on the occupied orbitals.[14a,c] Thus

$$\Delta\delta = \Delta\delta^p + \Delta\delta^d = \Delta\delta^{oc-vir} + \Delta\delta^{oc} \tag{5}$$

The components $\Delta\delta^{oc-vir}$ and $\Delta\delta^{oc}$ are displayed for carbon of the hexacarbonyls in Tables 6 and 7.

It is evident from these tables that $\Delta\delta^{oc-vir}$ is predominant (trend setting), and we have, in order to gain further insight into this term, decomposed it as[14c]

$$\Delta\delta^{oc-vir} = \frac{1}{3}\sum_{s=1}^{3}\Delta\delta^{dist}_{ss} + \frac{1}{3}\sum_{s=1}^{3}\Delta\delta^{p'}_{ss} \tag{6}$$

Here $\Delta\vec{\delta}^{dist} = \vec{\sigma}^{p'}_{CO} - \vec{\sigma}^{p'}_{CO*}$ is the change due to the elongation of the bond vector in CO to the distance it will have in the complex, CO*.

We display calculated values for $\Delta\delta^{dist}_{ss}$ ($s = x, y, z$) with respect to carbon in Tables 6 and 7, with the z axis pointing along the ^{13}CO bond vector. The negative paramagnetic shielding in CO is determined[14c] by the paramagnetic coupling between the σ_{CO} HOMO, **1a**, and the π^*_{CO} LUMO, **1b**, of CO through the overlaps $\langle\sigma_{CO}|\hat{M}_s|\pi^*_{CO}\rangle$ with $s = x, y$, where $\hat{M}_x\pi^*_{CO}$ is shown[20] in **1c**. It is, in addition, inversely proportional to the HOMO−LUMO energy gap $\Delta\epsilon_{HL}$. As the C−O distance

(20) The operation of $\hat{M}_s$ on an orbital is explained in ref 14c.

Table 7. Contribution to the Calculated Shift[a] in the Isotropic Shielding of ^{13}C for Complexed CO in $[M(CO)_6]^n$ for Various 3d and 4d Systems

system	$\Delta\delta_{xx}^{dist}$, ppm[b]	$\Delta\delta_{yy}^{dist}$, ppm[b]	$\Delta\delta_{zz}^{dist}$, ppm[b]	$\Delta\delta_{xx}^{p'}$, ppm[c]	$\Delta\delta_{yy}^{p'}$, ppm[c]	$\Delta\delta_{zz}^{p'}$, ppm[c]	$\Delta\delta^{oc}$, ppm[d]	$\Delta\delta^{oc-vir}$, ppm[e]	$\Delta\delta$, ppm[a]	energy gap, eV $2t_{2g} \rightarrow 2t_{1g}$
$Mo(CO)_6$[f,g]	9.4	9.4	0.0	−7.4	−7.4	31.1	3.8	11.7	15.5	5.214
$[Tc(CO)_6]^+$ [f]	5.3	5.3	0.0	−13.9	−13.9	17.5	5.0	0.1	5.1	6.195
$[Ru(CO)_6]^{2+}$ [f]	−0.3	−0.3	0.0	−27.9	−27.9	11.8	5.6	−14.8	−9.2	7.398
$Cr(CO)_6$[f,g]	7.2	7.2	0.0	3.2	3.2	35.7	0.5	18.8	19.3	5.592
$[Mn(CO)_6]^+$ [f]	6.1	6.1	0.0	−4.1	−4.1	24.8	0.5	9.6	10.2	6.528
$[Fe(CO)_6]^{2+}$ [f]	0.4	0.4	0.0	−19.0	−19.0	20.9	−0.1	−5.4	−5.5	7.519

[a−e] See Table 6. [f] No relativistic calculations. [g] Reference 14c.

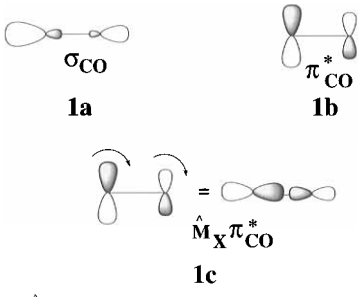

is stretched, the energy gap $\Delta\epsilon_{HL}$will decrease and the negative paramagnetic shielding will increase in absolute terms. It is thus clear that the term $\Delta\delta_{ss}^{dist}$ ($s = x, y$) increases linearly with R(C−O). For the negatively charged species $[Ta(CO)_6]^-$ and $[Hf(CO)_6]^{2-}$ with substantial π-back-donation and a stretched C−O bond, $\Delta\delta_{ss}^{dist}$ ($s = x, y$) is seen to afford a large positive contribution. As the π-back-donation diminishes and the C−O bond contracts toward more positively charged species in the 5d series, $\Delta\delta_{ss}^{dist}$ ($s = x, y$) becomes small and eventually negative when the C−O distance of the coordinated ligand is smaller than that of free ligand, Table 6. Quite similar trends are calculated for $\Delta\delta_{xx}^{dist}$ and $\Delta\delta_{yy}^{dist}$ in the 3d and 4d series.

The second part of eq 6 deals with the change in the coupling between occupied and virtual orbitals as CO* is complexed to the metal. The individual components of $\Delta\delta_{ss}^{p'}$ ($s = x, y, z$) can be found for carbon in Tables 6 and 7. The two components $\Delta\delta_{xx}^{p'}$ and $\Delta\delta_{yy}^{p'}$ are again determined by the paramagnetic coupling, **1c**, between the σ_{CO} HOMO, **1a**, and the π^*_{CO} LUMO, **1b**, of CO*. The σ_{CO} HOMO, **1a**, is now involved in the $2t_{1u}$, $1e_g$, and $1a_{1g}$ σ orbitals of the $M(CO)_6$ complex, Figure 1. They are all shifted to lower energy than σ_{CO} in free CO due to the bonding interactions with the $(n + 1)$s ($1a_{1g}$), nd_σ (e_g), and $(n + 1)$p ($2t_{1u}$) orbitals, Figure 1. The π^*_{CO} LUMO, **1b**, is on the other hand involved in the $2t_{1g}$, $3t_{1u}$, $2t_{2u}$, and $3t_{2g}$ orbitals of $M(CO)_6$, Figure 1. Of these, $3t_{2g}$ and $3t_{1u}$ are shifted to higher energies than π^*_{CO} of free CO due to interactions with metal orbitals. All these interactions widen the effective energy gap between σ_{CO} and π^*_{CO} with the result that the paramagnetic coupling is reduced and $\Delta\delta_{xx}^{p'}$ as well as $\Delta\delta_{yy}^{p'}$ is negative. It is thus understandable that the chemical shift is reduced, Tables 4 and 5, along with the coordination chemical shift, Tables 6 and 7, as the σ-donation becomes more important with increasing oxidation number of the metal center. The reduction is especially noticeable for the 5d series where the relativistic lowering of the 6s and 6p orbitals makes them more accessible for σ-donation interactions with σ_{CO}. This will result in a stabilization of $1a_{1g}$ and $3t_{2g}$, which will reduce the paramagnetic σ_{CO} to π^*_{CO} coupling. This reduction is primarily responsible for the fact that the coordination shifts $\Delta\delta$ of the 5d members are smaller than the corresponding shifts of the 4d and 3d homologues.

Table 8. A Correlation between $\Delta\delta_{zz}^{p'}$ and the Population[a] of π^*_{CO} in the 5d Metal Carbonyls, $[M(CO)_6]^n$

system	$\Delta\delta_{zz}^{p'}$ in ^{13}C, ppm	pop. of each π^*_{CO}	system	$\Delta\delta_{zz}^{p'}$ in ^{13}C, ppm	pop. of each π^*_{CO}
$[Hf(CO)_6]^{2-}$	103.6	0.32	$[Re(CO)_6]^+$	14.7	0.12
$[Ta(CO)_6]^-$	60.2	0.26	$[Os(CO)_6]^{2+}$	10.6	0.09
$W(CO)_6$	26.5	0.18	$[Ir(CO)_6]^{3+}$	5.8	0.05

[a] The total charge in each of the 12 π^*_{CO} orbitals contributing to the three $2t_{2g}$ HOMO's of Figure 1.

The complexed CO ligand has as opposed to free CO a paramagnetic contribution to the zz component of the shielding tensor in terms of $\Delta\delta_{zz}^{p'}$, Tables 6 and 7. There is one main category of coupling, and it involves the $2t_{2g}$ HOMO of the hexacarbonyl, **2a**, which is d_π based with an in-phase bonding

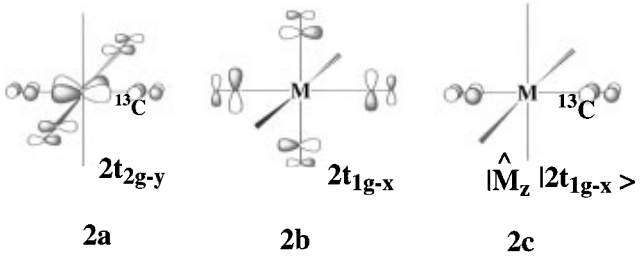

contribution from π^*_{CO}, and the empty $2t_{1g}$ orbitals, **2b**, which are purely π^*_{CO} based. Again, $\hat{M}_z|2t_{1g-x}\rangle$, **2c**, will overlap with $2t_{2g-y}$, **2a**, through the common π^*_{CO} lobes on **2a** and **2c**. The interaction between d_π and π^*_{CO} represents the back-donation of density from the metal to CO. We see that it tends to deshield ^{13}C by making a positive contribution to $\Delta\delta$, Tables 6 and 7. The term $\Delta\delta_{zz}^{p'}$ decreases from left to right along the transition series. This is because the energy gap between the $2t_{2g}$ HOMO orbitals and the empty $2t_{1g}$ orbitals increases, Table 6, and because the paramagnetic shielding is proportional to the inverse of the energy gap;[14a] the higher the gap, the lower the paramagnetic shielding. The paramagnetic coupling between the $2t_{2g}$ HOMO, **2a**, and the empty $2t_{1g}$ orbitals, **2b**, correlates with the bonding contributions from π^*_{CO} to the occupied d_π orbital since such contributions increase the coupling to the vacant π^*_{CO} combination. The correlation is illustrated in Table 8. The paramagnetic coupling in the case of $[Ir(CO)_6]^{3+}$ has the smallest value, 5.8 ppm, consistent with a small population of each π^*_{CO} in the HOMO, Table 8.

The picture that emerges from our analysis is that the metal to CO back-donation as well as the bond stretch of the coordinated CO ligand has a positive contribution to the coordination shift, $\Delta\delta$, for carbon whereas the contribution from the CO to metal donation is negative. With increasing oxidation of the metal, the σ-donation becomes more important and the

(21) (a) Oldfield, E.; Keniry, M. A.; Shinoda, S.; Schramm, S.; Broen, T.; Gutkowsky, H. S. *J. Chem. Soc., Chem. Commun.* **1985**, 791. (b) Gleeson, J. W.; Vaughan, R. W. *J. Chem. Phys.* **1983**, *78*, 5384.

π-back-donation less pronounced with the result that the chemical shift is diminished.

Conclusions

Molecular orbital calculations based on density functional theory have been carried out on the first CO bond dissociation energy as well as the vibrational frequencies and ^{13}C NMR chemical shift for the isoelectronic metal hexacarbonyls $[Hf(CO)_6]^{2-}$, $[Ta(CO)_6]^{-}$, $W(CO)_6$, $[Re(CO)_6]^{+}$, $[Os(CO)_6]^{2+}$, $[Ir(CO)_6]^{3+}$ and $Mo(CO)_6$, $[Tc(CO)_6]^{+}$, $[Ru(CO)_6]^{2+}$ as well as $Cr(CO)_6$, $[Mn(CO)_6]^{+}$, $[Fe(CO)_6]^{2+}$. We found in our theoretical study that the first ligand dissociation energy follows the ordering Cr $\sim$ Mn $<$ Fe for the 3d row, Mo $<$ Tc $<$ Ru for the 4d row, and Ir $>$ Re $\sim$ Os $>$ Hf $\sim$ Ta $\sim$ W, through the 5d row, primary as a result of a stronger σ-donation in the more oxidized systems.

Down the Mn and Fe triads, it is observed that the first ligand dissociation energy, ΔH, follows the ordering Tc $<$ Mn $<$ Re and Ru $<$ Fe $<$ Os with the 4d congener forming the most labile bond. This is because relativistic effects strengthen the M$-$CO bond by increasing the σ-CO donation. The same trend has been found[1b,c] in the case of the Cr triad, where ΔH follows the order Mo $<$ Cr $\sim$ W. However, in this case, the M$-$CO bond of the 5d congener is stabilized by an increase in the π-back-donation as the 5d orbitals are destabilized by relativity and thus more readily available to donate electrons.

The calculated vibrational CO stretching frequencies are in most cases within 10 cm^{-1} of experiment, with a maximum deviation of 46 cm^{-1}. Both calculated and observed CO stretching frequencies increase along a transition metal series with a corresponding increase of the formal charge of the metal. This is consistent with a corresponding decrease in π-back-bonding.

The ^{13}C chemical shift decreases along the 3d (Cr, Mn, Fe), 4d (Mo, Tc, Ru), and 5d (Hf, Ta, W, Re, Os) rows. The trends are due to a decrease in two positive and paramagnetic contributions to the chemical shift that diminish with respectively a reduction in π-back-donation and an increase in σ-donation. Within a triad, the chemical shift is decreasing as σ-donation becomes more important for the 5d congeners due to a relativistic stabilization of the 6s and 6p orbitals, which makes them more accessible as electron acceptors.

Acknowledgment. This work has been supported by the National Sciences and Engineering Research Council of Canada (NSERC). Y.R.-M. acknowledges a scholarship from DGAPA-UNAM (Mexico), and T.Z. acknowledges a Canada Council Killam Research Fellowship. Y.R.-M. is grateful to Dr. F. Aubke for providing ^{13}C NMR data and a preprint prior to publication. We thank the donors of the Petroleum Research Fund, administered by American Chemical Society (Grant ACS-PRF No. 31205-AC3), for further support of this research. A.W.E. was supported by the Deutsche Forschungsgemeinschaft (DFG) with a postdoctoral fellowship at the Vrije Universiteit. The foundation NCF is acknowledged for computer time, and the computational center SARA and the Holland Research School for Molecular Chemistry (HRSMC) enabled us to carry out calculations on parallel computer systems.

IC970223Z